International Journal of
Molecular Sciences

MDPI

Article

Interdomain Linker Effect on the Mechanical Stability of Ig Domains in Titin

Bei Tong [1], Fang Tian [2] and Peng Zheng [2,*]

[1] Institute of Botany, Jiangsu Province and Chinese Academy of Sciences, Nanjing 210014, China
[2] State Key Laboratory of Coordination Chemistry, Chemistry and Biomedicine Innovation Center (ChemBIC), School of Chemistry and Chemical Engineering, Nanjing University, Nanjing 210023, China
* Correspondence: pengz@nju.edu.cn

Abstract: Titin is the largest protein in humans, composed of more than one hundred immunoglobulin (Ig) domains, and plays a critical role in muscle's passive elasticity. Thus, the molecular design of this giant polyprotein is responsible for its mechanical function. Interestingly, most of these Ig domains are connected directly with very few interdomain residues/linker, which suggests such a design is necessary for its mechanical stability. To understand this design, we chose six representative Ig domains in titin and added nine glycine residues (9G) as an artificial interdomain linker between these Ig domains. We measured their mechanical stabilities using atomic force microscopy-based single-molecule force spectroscopy (AFM-SMFS) and compared them to the natural sequence. The AFM results showed that the linker affected the mechanical stability of Ig domains. The linker mostly reduces its mechanical stability to a moderate extent, but the opposite situation can happen. Thus, this effect is very complex and may depend on each particular domain's property.

Keywords: titin; force spectroscopy; interdomain linker

Citation: Tong, B.; Tian, F.; Zheng, P. Interdomain Linker Effect on the Mechanical Stability of Ig Domains in Titin. *Int. J. Mol. Sci.* **2022**, *23*, 9836. https://doi.org/10.3390/ijms23179836

Academic Editor: Yuri Lyubchenko

Received: 30 July 2022
Accepted: 26 August 2022
Published: 30 August 2022

1. Introduction

The giant muscle protein titin is a tandem modular construction designed polyprotein containing more than two hundred individually folded domains, such as immunoglobulin-like (Ig) and fibronectin-type III domains [1]. These domains are similar in size (~2 nm) and length (~90 residues). Interestingly, these domains are closely connected with very few residues in-between. Functionally, the I-band part of titin is extensible and plays a critical role in the passive elastic properties of muscles (Figure 1a). Thus, the molecular design for such a giant polyprotein is of great interest in understanding its mechanical function [2–5]. Here, we are particularly interested in whether the interdomain amino acid sequence/linker affects the mechanical stability of the Ig domains in titin, which has been studied with great interest [6–8].

To examine the linker effect, we used atomic force microscopy-based single-molecule force spectroscopy (AFM-SMFS) to measure the mechanical stability of human Ig domains. SMFS can manipulate a single molecule mechanically [9–22] and AFM-SMFS has been widely used to study the mechanical stability of proteins [23–29], protein-protein interactions [30–43], and chemical bonds [44–56]. Many titin domains have been studied [57–59]. For example, I27, the 27th Ig domain in titin (also called I91 based on a different nomenclature), is one of the first and most studied protein domains by AFM-SMFS, showing a force of ~200 pN and a contour length increment (ΔLc) of 28 nm upon unfolding [60]. In addition, the effect of the disulfide bond in I27 has been studied in detail [61,62].

Thus, we choose six consecutive Ig domains of titin, including I27, I28, I29, I30, I31, and I32, as a representative unit (I27–I31), to study the interdomain linker effect (Figure 1b). The structures and mechanical stabilities of many of these domains have been well determined. The crystal structure of I27 is available, while structures for other domains are constructed by the I-TASSER server (Figure 1b). It is noted that I27 is a historical nomenclature,

especially in the AFM-SMFS field, and we used it here. It is renamed I91 later [63]. There are 89 extensible residues in each Ig domain except for I30, leading to ΔLc of ~28 nm, as shown for I27. For I30, a disulfide bond may be formed between the Cys23 and Cys73, leading to a smaller ΔLc with only 51 extensible residues (Figure 1c). In addition, we designed nine glycines (9G) as an artificial linker due to its simple structure without a self-secondary structure.

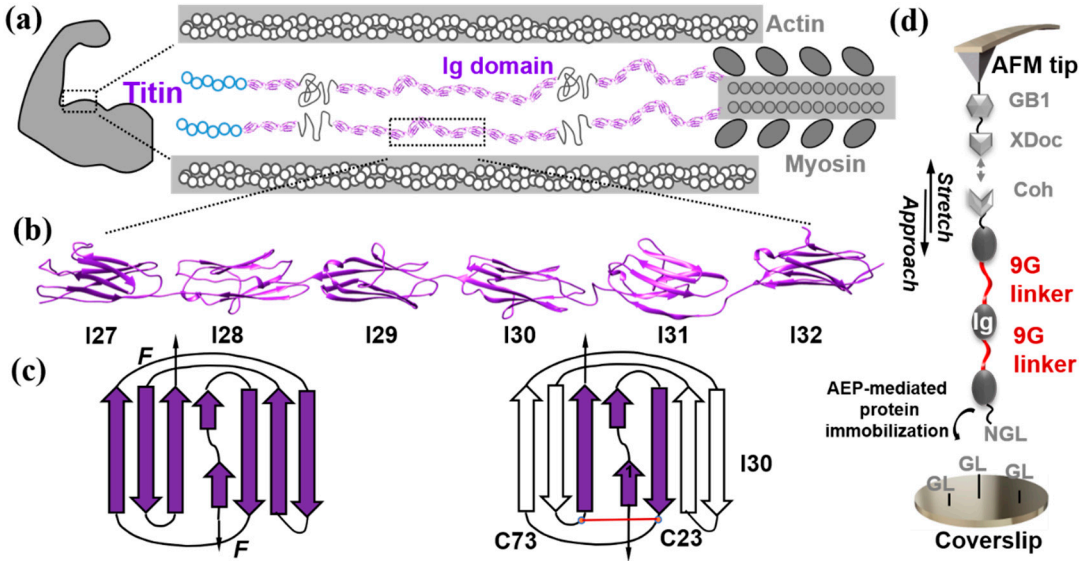

Figure 1. (**a**) Schematic architecture of one-half of the sarcomere highlights the polyprotein structure of giant protein titin (colored in purple), not in scale. (**b**) Structure shows human titin segment I(27–32) chosen for mechanical stability measurements. Except for I27 (PDB:1TIT), all others are simulated structures. (**c**) The cartoon shows the structure of I30 with a possible disulfide bond between Cys73 and Cys23, while no disulfide is present in other Ig domains. (**d**) The schematic shows how high-precision AFM-SMFS measures the mechanical stability of Ig domains with an artificial linker.

2. Results

A high-precision AFM measurement system has been used for accurate measurement and comparison of Ig domains in titin [64–67] (Figure 1d). In short, the target polyprotein designed with a specific peptide sequence NGL was immobilized on a GL peptide-coated surface through AEP (asparaginyl endopeptidase)-mediated protein ligation between the two peptide sequences [68]. A GB1-XDoc coated-AFM tip was used to probe the target polyprotein (Figure 2c). Here, GB1 with known properties (Force = 180 pN, ΔLc = 18 nm) was added, serving as an internal force caliper [69]. The reversible protein-protein interaction Cohesion:XDockerin (Coh:XDoc) was used to enable efficient protein pick-up [64].

Thus, we built polyprotein Coh-I(27–32)/9G-NGL with a 9G linker for measurement. The 9G linker is present between each Ig domain except for the two end I27 and I32 domains (Figure 2a). By approaching the AFM tip towards the surface, the polyprotein was picked up between the Coh:XDoc interaction. Upon stretching, the polyprotein was under mechanical manipulation and its corresponding force-extension curve showed characteristic sawtooth-like peaks from the stepwise unfolding of each domain, and a final rupture peak with a higher force of ~600 pN was observed from the break of Coh:XDoc complex. By fitting the elasticity of the curve using the worm-like chain model [70], five unfolding events from Ig domains were obtained, showing a ΔLc of 28 ± 2 nm (Figure 2b), agreeing well with the theoretical value. Moreover, the unfolding forces of different Ig domains are similar. The force histogram showed a single peak with an average unfolding force of 308 ± 64 pN (ave. + stdv. n = 1148, Figure 2c). Besides, an additional peak with a ΔLc of 11 ± 2 nm was observed, which was from the partial unfolding of I30 (Figure 1c). As described, a

disulfide bond is indeed presented in I30. Thus, only 40 residues can be unfolded, leading to a theoretical value of 10.4 nm (40 × 0.36 − 4.0 nm).

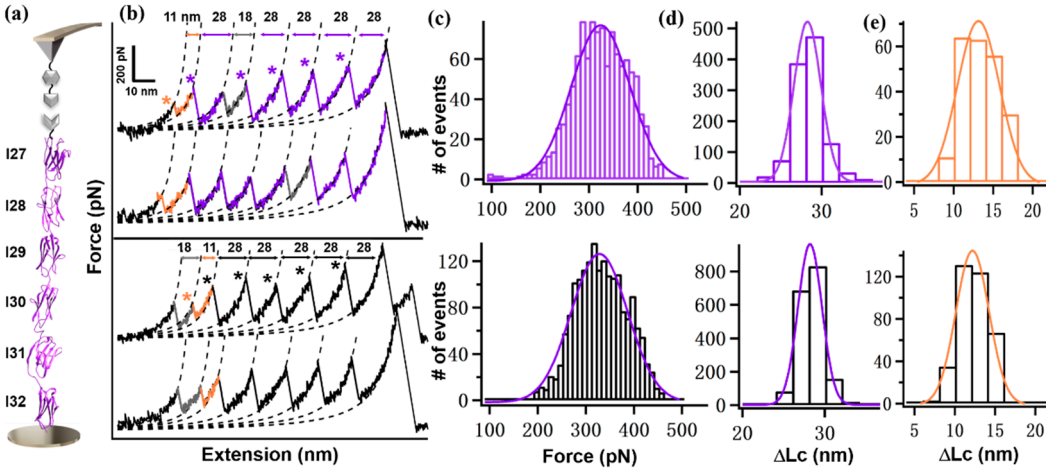

Figure 2. (**a**) Scheme of AFM-SMFS setup to measure the mechanical stability of polyprotein I(27–32). (**b**) Representative force-extension curves show the unfolding events of Ig domains (marked by a star). The top two curves are from the unfolding of polyprotein with an artificial 9G linker (colored in purple) and the bottom curves are from the natural polyprotein sequence without the linker. The I30 domain shows a peak with ΔLc of 11 nm (in orange), the remaining five Ig domains all show a peak with ΔLc of 28 nm, and GB1 shows a ΔLc of 18 nm. (**c**,**d**) Histograms show the unfolding force (**c**) and ΔLc (**d**) from the five Ig domains. (**e**) The histogram shows the ΔLc of I30.

Then, we used polyprotein Coh-I(27–32)-NGL with natural sequence for AFM measurement and comparison. The same cantilever used previously for the polyprotein with the linker was used here again to minimize the error. As expected, a similar unfolding pattern was observed (Figure 2b,d,e). However, the force is slightly lower, with a value of 324 ± 54 pN (*n* = 1808, Figure 2c) (Table 1).

Table 1. Unfolding force of Ig domains for each polyprotein design.

Polyprotein	9G Linker	No Linker
I(27–32)	308 ± 64 pN (*n* = 1148)	324 ± 54 pN (*n* = 1808)
I(28–30)	325 ± 35 pN (*n* = 965)	330 ± 36 pN (*n* = 860)
I(30–32)	320 ± 33 pN (*n* = 1120)	276 pN/345 pN (*n* = 1804)

To confirm this effect, we chose three Ig domains only and constructed two shorter polyproteins, Coh-I(28–30)/9G-NGL and Coh-I(30–32)/9G-NGL, for measurement. Indeed, stretching these polyproteins resulted in a shorter force-extension curve with only two 28 nm-peaks from I28, I29, or I31, I32, and one 11 nm-peak from I30, as expected (Figures 3 and 4). For Coh-I(28–30)/9G-NGL, the histogram of unfolding forces from I28 and I29 showed a single peak with an average force of 330±36 pN (*n* = 860). Then, AFM measurement on Coh-I(28–30)-NGL with natural sequence showed a force of 325 ± 35 pN (*n* = 965).

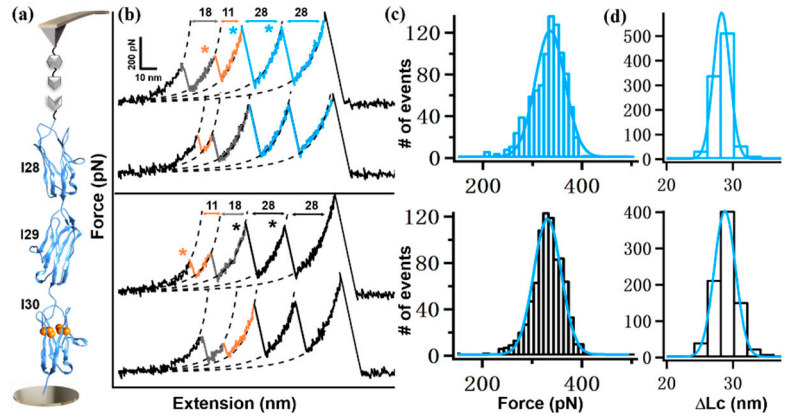

Figure 3. (**a**) Scheme of AFM-SMFS setup to measure I(28–30) domains. (**b**) Representative force-extension curves from polyprotein with linkers (top, colored in blue) and without linker (bottom, black). (**c**,**d**) Histograms of their corresponding unfolding force (**c**) and ΔLc (**d**) are shown. The star indicates the unfolding event/peak of one protein domain.

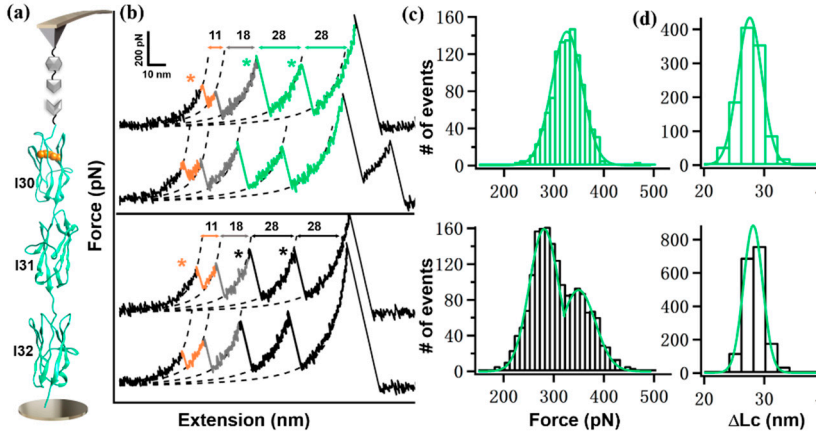

Figure 4. (**a**) Scheme of AFM-SMFS setup to measure I(30–32) domains. (**b**) Representative force-extension curves from polyprotein with linkers (top, colored in green) and without linker (bottom, in black). (**c**,**d**) Histograms of their corresponding unfolding force (**c**) and ΔLc (**d**) are shown. The star indicates the unfolding event/peak.

For Coh-I(30–32)/9G-NGL, the histogram of unfolding force from I31 and I32 showed a single peak with an average force of 320 ± 33 pN (n = 1120). However, AFM measurement on the natural sequence showed a different result. Two peaks were observed in the histogram, with a force of 276 pN and 345 pN, respectively (n = 1804), which has not been observed before.

As a result, the unfolding force of Ig domains in titin is generally lower when the 9-glycine length amino acids sequence is present as an interdomain linker. Moreover, the effect can be complex when considering the unfolding force of I31 and I32.

Finally, we focused on the unfolding results of I30 in each polyprotein design. First, with an internal disulfide bond, I30 showed a unique 11 nm-peak which can be distinguished from other Ig domains. Thus, its unfolding force can be assigned unambiguously. Moreover, the linker situation for I30 in the three polyproteins is different (Figure 5). For I(27–32), 9G linker is present on both sides of I30 (Figure 5a). In this design, the unfolding force of I30 was 203 ± 34 pN (n = 360), and 186 ± 55 pN (n = 225) without linker. For I(28–30), 9G linker is only present on the N terminus. The force was 197 pN (n = 570), and 172 ± 24 pN (n = 910) without linker. Finally, for I(30–32), 9G linker is only present on the C terminus. The force was 159 ± 23 pN (n = 477), and 175 ± 24 pN (n = 404) without the linker (Table 2).

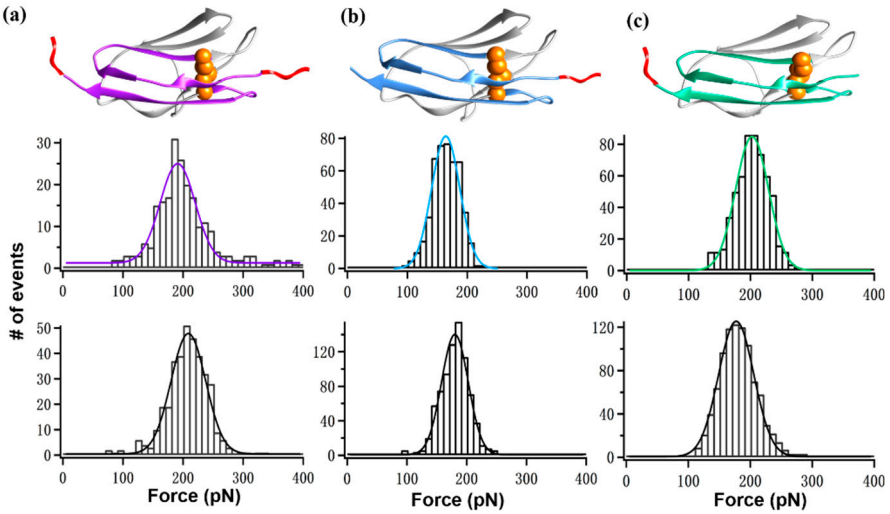

Figure 5. (**a**–**c**) The scheme (top panel) and mechanical force of I30 in polyprotein I(27–32) (**a**), I(28–30) (**b**), and I(30–32) (**c**). The unfolding force histogram of I30 with the corresponding linker is shown in the middle panel, and the natural sequence without linker is shown at the bottom. The 9G linker was colored red, and the two cysteines forming the disulfide bond were depicted as orange spheres.

Table 2. Unfolding force of I30 in each polyprotein design.

Polyprotein	9G Linker	No Linker
I(27–32)	186 ± 55 pN (*n* = 225)	203 ± 34 pN (*n* = 360)
I(28–30)	159 ± 23 pN (*n* = 477)	175 ± 24 pN (*n* = 404)
I(30–32)	197 ± 26 pN (*n* = 570)	172 ± 30 pN (*n* = 910)

Based on these results for I30, we found that this linker effect is much more complex than we thought before. Indeed, a few cases have been studied for the linker effect, both mechanically and thermodynamically [71,72]. No general trend/conclusion has been obtained. In this work, we found the linker can reduce the mechanical stability of I30 when present in I(27–32) and I(30–32) while increasing it when present in I(28–30). Nevertheless, it is no doubt that the linker affects the domain stability in titin.

In this work, we determined the effect of the interdomain linker for the Ig domain in titin. By measuring the mechanical stability of polyprotein containing multiple Ig domains in titin, with/without an artificial 9G linker, we found the linker indeed affects the Ig domain's stability. The force is reduced when an artificial linker is present in most cases. However, the extent can vary; sometimes the trend is reversed. Thus, we believe this linker effect is much more complex, and the intrinsic property of each domain and the linker itself play important roles. Nevertheless, this work provides a glimpse of the molecular design of the giant titin, and future studies are needed to understand this important molecule for humans and even for designing artificial muscle [73–75].

3. Method and Material

Protein engineering: The plasmid: Coh-I(27–32)/9G-NGL, Coh-I(27–32)-NGL, Coh-I(28–30)/9G-NGL, Coh-I(28–30)-NGL, Coh-I(30–32)/9G-NGL, Coh-I(30–32)-NGL were obtained after Gibson assembly-based method [76]. All plasmids were overexpressed in *Escherichia coli* strain BL21 (DE3) and cells were cultured overnight in LB medium at 18 °C by the addition of 1mM IPTG. The cells were pelleted by centrifugation and the polyprotein purification by Ni-NTA affinity. After using wash buffer (50 mM Tris, 100 mM NaCl, 20 mM imidazole, pH 7.4) to purify the target proteins, the polyproteins were eluted in elution buffer (50 mM Tris, 100 mM NaCl, 200 mM imidazole, pH 7.4). Protein ligase AEP was obtained according to literature [77].

Protein immobilization: The glass coverslips (Sail Brand, China) and probes (MLCT-Bio-DC, Bruker) were cleaned by plasma. Then, both probes and coverslips were immersed in 1% (*v/v*) APTES toluene solution for 1 h to add the NH_2 group, followed by a reaction with Milli-Q water containing 2 mM $ImSO_2N_3$, 4 mM K_2CO_3, and 20 mM $CuSO_4$ to add the N_3 group. After flushing, they were further reacted with DBCO-PEG_4-maleimide for at least 2 h to add the maleimide group. Peptide C-ELP_{20}-NGL and GL-ELP_{20}-C were respectively reacted onto the probe and coverslip. For AFM-SMFS measurement, 50 µL AFM buffer (100 mM Tris, 100 mM NaCl, pH 7.4) containing 100 µM Ig proteins and 50 µM AEP were pipetted on the glass slides for 40 min. The cantilevers were incubated with 50 µL solution of 60 µM GL-CBM-XDoc and 50 Mm AEP in the AFM buffer.

AFM-SMFS Experiment: Measurements using Coh-Doc interaction of high rupture force as a standard were carried out Nanowizard4 (JPK) atomic force microscope. Using the equipartition theorem, the spring constant of ~30 pN nm^{-1} was obtained by calibrating the MLCT-Bio-DC (Bruker) cantilever in the AFM buffer solution. The functionalized cantilevers and glass coverslip immobilize polyproteins in AFM buffer at pH 7.4. All AFM experiments were performed at a constant pulling speed of 1000 $nm{\cdot}s^{-1}$.

Protein sequence (I27-**9G**-I28-**9G**-I29-**9G**-I30-**9G**-I31-**9G**-I32)

LIEVEKPLYGVEVFVGETAHFEIELSEPDVHGQWK-
LKGQPLAASPDCEIIEDGKKHILILHNCQLGMTGEV-
SFQAANTKSAANLKVKEL**GGGGGGGGG**PL-
IFITPLSDVKVFEKDEAKFECEVSREPKTFRWLKGTQ-
EITGDDRFELIKDGTKHSMVIKSAAFEDEAKYMFEAE-
DKHTSGKLIIEGI**GGGGGGGGG**RLKFL-
TPLKDVTAKEKESAVFTVELSHDNIRVKWFKNDQRLHT-
TRSVSMQDEGKTHSITFKDLSIDDTSQIRVEAMGMSSEA-
KLTVLEG**GGGGGGGGG**DPYFT-
GKLQDYTGVEKDEVILQCEISKADAPVKWFKDGKEIKPSK-
NAVIKTDGKKRMLILKKALKSDIGQYTCDCGTDKTSGKLD-
IEDR**GGGGGGGGG**EIKLVRPLHS-
VEVMETETARFETEISEDDIHANWKLKGEALLQTPDCEIKEE-
GKIHSLVLHNCRLDQTGGVDFQAANVKSSAHL-
RVKPR**GGGGGGGGG**VIGLLRPLKDVTVTA-
GETATFDCELSYEDIPVEWYLKGKKLEPSDKVVPRSEGKVHT-
LTLRDVKLEDAGEVQLTAKDFKTHANLFVKEP

Author Contributions: Conceptualization, P.Z. and B.T.; methodology, P.Z. and F.T.; investigation, B.T. and F.T.; P.Z. and B.T.—original draft preparation, P.Z. and B.T.; writing—review and editing; funding acquisition, P.Z. and B.T. All authors have read and agreed to the published version of the manuscript.

Funding: This work was funded by Natural Science Foundation of Jiangsu Province No. BK20200058 (P.Z.), No. BK20190275 (B.T.), and No. BK20202004 (P.Z.), Fundamental Research Funds for the Central Universities 14380205 (P.Z.), and National Natural Science Foundation of China grant No. 21977047 (P.Z.).

Data Availability Statement: Data is contained within the article.

Conflicts of Interest: The authors declare no conflict of interest.

References

1. Labeit, S.; Kolmerer, B. Titins: Giant proteins in charge of muscle ultrastructure and elasticity. *Science* **1995**, *270*, 293–296. [CrossRef]
2. Wang, R.; Li, J.; Li, X.; Guo, J.; Liu, J.; Li, H. Engineering protein polymers of ultrahigh molecular weight via supramolecular polymerization: Towards mimicking the giant muscle protein titin. *Chem. Sci.* **2019**, *10*, 9277–9284. [CrossRef] [PubMed]
3. Li, H.B.; Linke, W.A.; Oberhauser, A.F.; Carrion-Vazquez, M.; Kerkviliet, J.G.; Lu, H.; Marszalek, P.E.; Fernandez, J.M. Reverse engineering of the giant muscle protein titin. *Nature* **2002**, *418*, 998–1002. [CrossRef] [PubMed]

4. Suay-Corredera, C.; Pricolo, M.R.; Velazquez-Carreras, D.; Pathak, D.; Nandwani, N.; Pimenta-Lopes, C.; Sanchez-Ortiz, D.; Urrutia-Irazabal, I.; Vilches, S.; Dominguez, F.; et al. Nanomechanical phenotypes in cardiac myosin-binding protein c mutants that cause hypertrophic cardiomyopathy. *ACS Nano* **2021**, *15*, 10203–10216. [CrossRef] [PubMed]
5. Wang, D.; Marszalek, P.E. Exploiting a mechanical perturbation of a titin domain to identify how force field parameterization affects protein refolding pathways. *J. Chem. Theory Comput.* **2020**, *16*, 3240–3252. [CrossRef] [PubMed]
6. Zacharchenko, T.; von Castelmur, E.; Rigden, D.J.; Mayans, O. Structural advances on titin: Towards an atomic understanding of multi-domain functions in myofilament mechanics and scaffolding. *Biochem. Soc. Trans.* **2015**, *43*, 850–855. [CrossRef]
7. Fleming, J.R.; Rigden, D.J.; Mayans, O. The importance of chain context in assessing small nucleotide variants in titin: In silico case study of the i10-i11 tandem and its arrhythmic right ventricular cardiomyopathy linked position t2580. *J. Biomol. Struct. Dyn.* **2021**, *39*, 3480–3490. [CrossRef]
8. Lanzicher, T.; Zhou, T.; Saripalli, C.; Keschrumrus, V.; Smith Iii, J.E.; Mayans, O.; Sbaizero, O.; Granzier, H. Single-molecule force spectroscopy on the n2a element of titin: Effects of phosphorylation and carp. *Front. Physiol.* **2020**, *11*, 173. [CrossRef]
9. Zhang, W.; Hou, J.; Li, N.; Zhang, W.K. Application of atomic force microscopy (AFM)-based single-molecule force spectroscopy (SMFS) in polymer characterization. *Acta Polym. Sin.* **2021**, *52*, 1523–1546.
10. Bao, Y.; Huang, X.; Xu, J.; Cui, S. Effect of intramolecular hydrogen bonds on the single-chain elasticity of poly(vinyl alcohol): Evidencing the synergistic enhancement effect at the single-molecule level. *Macromolecules* **2021**, *54*, 7314–7320. [CrossRef]
11. Hao, X.; Zhang, J.; Yang, Y.; Wang, H.; Chi, Q. Single-molecule interactions between heme proteins and carboxylic groups in various chemical environments. *Chemelectrochem* **2020**, *7*, 4441–4445. [CrossRef]
12. Le, S.; Yu, M.; Yan, J. Direct single-molecule quantification reveals unexpectedly high mechanical stability of vinculin-talin/alpha-catenin linkages. *Sci. Adv.* **2019**, *5*, eaav2720. [CrossRef]
13. Koo, H.; Park, I.; Lee, Y.; Kim, H.J.; Jung, J.H.; Lee, J.H.; Kim, Y.; Kim, J.H.; Park, J.W. Visualization and quantification of microrna in a single cell using atomic force microscopy. *J. Am. Chem. Soc.* **2016**, *138*, 11664–11671. [CrossRef] [PubMed]
14. Zhao, M.; Woodside, M.T. Mechanical strength of RNA knot in zika virus protects against cellular defenses. *Nat. Chem. Biol.* **2021**, *17*, 975–981. [CrossRef] [PubMed]
15. Tapia-Rojo, R.; Alonso-Caballero, A.; Fernandez, J.M. Talin folding as the tuning fork of cellular mechanotransduction. *Proc. Natl. Acad. Sci. USA* **2020**, *117*, 21346–21353. [CrossRef] [PubMed]
16. Alonso-Caballero, A.; Echelman, D.J.; Tapia-Rojo, R.; Haldar, S.; Eckels, E.C.; Fernandez, J.M. Protein folding modulates the chemical reactivity of a gram-positive adhesin. *Nat. Chem.* **2021**, *13*, 172–181. [CrossRef] [PubMed]
17. Rico-Pasto, M.; Alemany, A.; Ritort, F. Force-dependent folding kinetics of single molecules with multiple intermediates and pathways. *J. Phys. Chem. Lett.* **2022**, *13*, 1025–1032. [CrossRef]
18. Rissone, P.; Bizarro, C.V.; Ritort, F. Stem loop formation drives rna folding in mechanical unzipping experiments. *Proc. Natl. Acad. Sci. USA* **2022**, *119*, e2025575119. [CrossRef]
19. Zhang, X.; Kou, X.; Zhang, W.; Zhang, W. Identification of the new type of g-quadruplex with multiple vacant sites in human telomeric DNA. *CCS Chem.* **2021**, *3*, 3192–3204. [CrossRef]
20. Ma, L.; Xu, M.; Oberhauser, A.F. Naturally occurring osmolytes modulate the nanomechanical properties of polycystic kidney disease domains. *J. Biol. Chem.* **2010**, *285*, 38438–38443. [CrossRef]
21. Bustamante, C.J.; Chemla, Y.R.; Liu, S.; Wang, M.D. Optical tweezers in single-molecule biophysics. *Nat. Rev. Methods Primers* **2021**, *1*, 25. [CrossRef] [PubMed]
22. Lu, S.; Cai, W.; Cao, N.; Qian, H.-J.; Lu, Z.-Y.; Cui, S. Understanding the extraordinary flexibility of polydimethylsiloxane through single-molecule mechanics. *ACS Mater. Lett.* **2022**, *4*, 329–335. [CrossRef]
23. Liu, Z.; Moreira, R.A.; Dujmović, A.; Liu, H.; Yang, B.; Poma, A.B.; Nash, M.A. Mapping mechanostable pulling geometries of a therapeutic anticalin/ctla-4 protein complex. *Nano Lett.* **2021**, *22*, 179–181. [CrossRef] [PubMed]
24. Wang, H.; Gao, X.; Li, H. Single molecule force spectroscopy reveals the mechanical design governing the efficient translocation of the bacterial toxin protein rtx. *J. Am. Chem. Soc.* **2019**, *141*, 20498–20506. [CrossRef] [PubMed]
25. Wolny, M.; Batchelor, M.; Bartlett, G.J.; Baker, E.G.; Kurzawa, M.; Knight, P.J.; Dougan, L.; Takagi, Y.; Woolfson, D.N.; Paci, E.; et al. Design and characterization of long and stable de novo single alpha-helix domains. *Biophys. J.* **2017**, *112*, 189a. [CrossRef]
26. Arora, N.; Hazra, J.P.; Rakshit, S. Anisotropy in mechanical unfolding of protein upon partner-assisted pulling and handle-assisted pulling. *Commun. Biol.* **2021**, *4*, 925. [CrossRef]
27. Brockwell, D.J.; Paci, E.; Zinober, R.C.; Beddard, G.S.; Olmsted, P.D.; Smith, D.A.; Perham, R.N.; Radford, S.E. Pulling geometry defines the mechanical resistance of a beta-sheet protein. *Nat. Struct. Biol.* **2003**, *10*, 731–737. [CrossRef]
28. Takahashi, H.; Rico, F.; Chipot, C.; Scheuring, S. Alpha-helix unwinding as force buffer in spectrins. *ACS Nano* **2018**, *12*, 2719–2727. [CrossRef]
29. Ding, Y.; Apostolidou, D.; Marszalek, P. Mechanical stability of a small, highly-luminescent engineered protein nanoluc. *Int. J. Mol. Sci.* **2021**, *22*, 55. [CrossRef]
30. Zhang, X.; Rico, F.; Xu, A.; Moy, V. Atomic force microscopy of protein-protein interactions. In *Handbook of Single-Molecule Biophysics*; Hinterdorfer, P., Oijen, A., Eds.; Springer: New York, NY, USA, 2009; pp. 555–570.
31. Tian, F.; Tong, B.; Sun, L.; Shi, S.; Zheng, B.; Wang, Z.; Dong, X.; Zheng, P. N501y mutation of spike protein in SARS-CoV-2 strengthens its binding to receptor ace2. *Elife* **2021**, *10*, e69091. [CrossRef]

32. Hinterdorfer, P.; Baumgartner, W.; Gruber, H.J.; Schilcher, K.; Schindler, H. Detection and localization of individual antibody-antigen recognition events by atomic force microscopy. *Proc. Natl. Acad. Sci. USA* **1996**, *93*, 3477–3481. [CrossRef]
33. Oh, Y.J.; Kohler, M.; Lee, Y.; Mishra, S.; Park, J.W.; Hinterdorfer, P. Label-free probing of binding affinity using topography and recognition imaging. *Biophys. J.* **2020**, *118*, 174a–175a. [CrossRef]
34. Cao, W.; Dong, C.; Kim, S.; Hou, D.; Tai, W.; Du, L.; Im, W.; Zhang, X.F. Biomechanical characterization of SARS-CoV-2 spike rbd and human ace2 protein-protein interaction. *Biophys. J.* **2021**, *120*, 1011–1019. [CrossRef] [PubMed]
35. Bauer, M.S.; Gruber, S.; Hausch, A.; Gomes, P.; Milles, L.F.; Nicolaus, T.; Schendel, L.C.; Navajas, P.L.; Procko, E.; Lietha, D.; et al. A tethered ligand assay to probe sars-cov-2:Ace2 interactions. *Proc. Natl. Acad. Sci. USA* **2022**, *119*, e2114397119. [CrossRef] [PubMed]
36. Zhang, X.; Chen, J.; Li, E.; Hu, C.; Luo, S.Z.; He, C. Ultrahigh adhesion force between silica-binding peptide sb7 and glass substrate studied by single-molecule force spectroscopy and molecular dynamic simulation. *Front. Chem.* **2020**, *8*, 600918. [CrossRef]
37. Wojcikiewicz, E.P.; Abdulreda, M.H.; Zhang, X.H.; Moy, V.T. Force spectroscopy of lfa-1 and its ligands, icam-1 and icam-2. *Biomacromolecules* **2006**, *7*, 3188–3195. [CrossRef]
38. Wang, Y.J.; Rico-Lastres, P.; Lezamiz, A.; Mora, M.; Solsona, C.; Stirnemann, G.; Garcia-Manyes, S. DNA binding induces a nanomechanical switch in the rrm1 domain of tdp-43. *J. Phys. Chem. Lett.* **2018**, *9*, 3800–3807. [CrossRef]
39. Milles, L.F.; Schulten, K.; Gaub, H.E.; Bernardi, R.C. Molecular mechanism of extreme mechanostability in a pathogen adhesin. *Science* **2018**, *359*, 1527–1533. [CrossRef]
40. Prescilla-Ledezma, A.; Linares, F.; Ortega-Muñoz, M.; Retana Moreira, L.; Jódar-Reyes, A.B.; Hernandez-Mateo, F.; Santoyo-Gonzalez, F.; Osuna, A. Molecular recognition of surface trans-sialidases in extracellular vesicles of the parasite trypanosoma cruzi using atomic force microscopy (afm). *Int. J. Mol. Sci.* **2022**, *23*, 7193. [CrossRef]
41. Lipke, P.N.; Rauceo, J.M.; Viljoen, A. Cell-cell mating interactions: Overview and potential of single-cell force spectroscopy. *Int. J. Mol. Sci.* **2022**, *23*, 1110. [CrossRef]
42. Yang, J.; Petitjean, S.J.L.; Koehler, M.; Zhang, Q.; Dumitru, A.C.; Chen, W.; Derclaye, S.; Vincent, S.P.; Soumillion, P.; Alsteens, D. Molecular interaction and inhibition of SARS-CoV-2 binding to the ace2 receptor. *Nat. Commun.* **2020**, *11*, 4541. [CrossRef] [PubMed]
43. Liu, Y.; Tian, F.; Shi, S.; Deng, Y.; Zheng, P. Enzymatic protein–protein conjugation through internal site verified at the single-molecule level. *J. Phys. Chem. Lett.* **2021**, *12*, 10914–10919. [CrossRef] [PubMed]
44. Yuan, G.; Curtolo, F.; Deng, Y.; Wu, T.; Tian, F.; Ma, Q.; Liu, Y.; Zuo, J.; Arantes, G.M.; Zheng, P. Highly dynamic polynuclear metal cluster revealed in a single metallothionein molecule. *Research* **2021**, *2021*, 9756945. [CrossRef] [PubMed]
45. Pill, M.F.; East, A.L.L.; Marx, D.; Beyer, M.K.; Clausen-Schaumann, H. Mechanical activation drastically accelerates amide bond hydrolysis, matching enzyme activity. *Angew. Chem. Int. Ed.* **2019**, *58*, 9787–9790. [CrossRef]
46. Zhao, P.; Xu, C.-Q.; Sun, C.; Xia, J.; Sun, L.; Li, J.; Xu, H. Exploring the difference of bonding strength between silver(i) and chalcogenides in block copolymer systems. *Polym. Chem.* **2020**, *11*, 7087–7093. [CrossRef]
47. Lei, H.; Ma, Q.; Li, W.; Wen, J.; Ma, H.; Qin, M.; Wang, W.; Cao, Y. An ester bond underlies the mechanical strength of a pathogen surface protein. *Nat. Commun.* **2021**, *12*, 5082. [CrossRef]
48. López-García, P.; de Araujo, A.D.; Bergues-Pupo, A.E.; Tunn, I.; Fairlie, D.P.; Blank, K.G. Fortified coiled coils: Enhancing mechanical stability with lactam or metal staples. *Angew. Chem. Int. Ed.* **2021**, *60*, 232–236. [CrossRef]
49. Xiang, W.; Li, Z.; Xu, C.-Q.; Li, J.; Zhang, W.; Xu, H. Quantifying the bonding strength of gold-chalcogen bonds in block copolymer systems. *Chem. Asian J.* **2019**, *14*, 1481–1486. [CrossRef] [PubMed]
50. Nie, J.; Deng, Y.; Tian, F.; Shi, S.; Zheng, P. Detection of weak non-covalent cation-π interactions in ngal by single-molecule force spectroscopy. *Nano Res.* **2022**, *15*, 4251–4257. [CrossRef]
51. Rico, F.; Russek, A.; Gonzalez, L.; Grubmuller, H.; Scheuring, S. Heterogeneous and rate-dependent streptavidin-biotin unbinding revealed by high-speed force spectroscopy and atomistic simulations. *Proc. Natl. Acad. Sci. USA* **2019**, *116*, 6594–6601. [CrossRef]
52. Nie, J.Y.; Tian, F.; Zheng, B.; Wang, Z.Y.; Zheng, P. Exploration of metal-ligand coordination bonds in proteins by single-molecule force spectroscopy. *Chem. Lett.* **2021**, *50*, 1667–1675. [CrossRef]
53. Nunes-Alves, A.; Arantes, G.M. Mechanical unfolding of macromolecules coupled to bond dissociation. *J. Chem. Theory Comput.* **2018**, *14*, 282–290. [CrossRef] [PubMed]
54. Li, S.; Pang, X.; Zhao, J.; Zhang, Q.; Shan, Y. Evaluating the single-molecule interactions between targeted peptides and the receptors on living cell membrane. *Nanoscale* **2021**, *13*, 17318–17324. [CrossRef] [PubMed]
55. Razgoniaev, A.O.; Glasstetter, L.M.; Kouznetsova, T.B.; Hall, K.C.; Horst, M.; Craig, S.L.; Franz, K.J. Single-molecule activation and quantification of mechanically triggered palladium–carbene bond dissociation. *J. Am. Chem. Soc.* **2021**, *143*, 1784–1789. [CrossRef]
56. Song, G.; Tian, F.; Liu, H.; Li, G.; Zheng, P. Pioglitazone inhibits metal cluster transfer of mitoneet by stabilizing the labile Fe–N bond revealed at single-bond level. *J. Phys. Chem. Lett.* **2021**, *12*, 3860–3867. [CrossRef]
57. Pang, S.M.; Le, S.; Yan, J. Mechanical responses of the mechanosensitive unstructured domains in cardiac titin. *Biol. Cell* **2018**, *110*, 65–76. [CrossRef]
58. Yuan, G.; Le, S.; Yao, M.; Qian, H.; Zhou, X.; Yan, J.; Chen, H. Elasticity of the transition state leading to an unexpected mechanical stabilization of titin immunoglobulin domains. *Angew. Chem. Int. Ed.* **2017**, *56*, 5490–5493. [CrossRef]

59. Williams, P.M.; Fowler, S.B.; Best, R.B.; Luis Toca-Herrera, J.; Scott, K.A.; Steward, A.; Clarke, J. Hidden complexity in the mechanical properties of titin. *Nature* **2003**, *422*, 446. [CrossRef]
60. Carrion-Vazquez, M.; Oberhauser, A.F.; Fowler, S.B.; Marszalek, P.E.; Broedel, S.E.; Clarke, J.; Fernandez, J.M. Mechanical and chemical unfolding of a single protein: A comparison. *Proc. Natl. Acad. Sci. USA* **1999**, *96*, 3694–3699. [CrossRef]
61. Giganti, D.; Yan, K.; Badilla, C.L.; Fernandez, J.M.; Alegre-Cebollada, J. Disulfide isomerization reactions in titin immunoglobulin domains enable a mode of protein elasticity. *Nat. Commun.* **2018**, *9*, 185. [CrossRef]
62. Popa, I.; Kosuri, P.; Alegre-Cebollada, J.; Garcia-Manyes, S.; Fernandez, J.M. Force dependency of biochemical reactions measured by single-molecule force-clamp spectroscopy. *Nat. Protoc.* **2013**, *8*, 1261–1276. [CrossRef] [PubMed]
63. Bang, M.-L.; Centner, T.; Fornoff, F.; Geach, A.J.; Gotthardt, M.; McNabb, M.; Witt, C.C.; Labeit, D.; Gregorio, C.C.; Granzier, H.; et al. The complete gene sequence of titin, expression of an unusual 700-KDa titin isoform, and its interaction with obscurin identify a novel z-line to i-band linking system. *Circ. Res.* **2001**, *89*, 1065–1072. [CrossRef] [PubMed]
64. Stahl, S.W.; Nash, M.A.; Fried, D.B.; Slutzki, M.; Barak, Y.; Bayer, E.A.; Gaub, H.E. Single-molecule dissection of the high-affinity cohesin-dockerin complex. *Proc. Natl. Acad. Sci. USA* **2012**, *109*, 20431–20436. [CrossRef]
65. Deng, Y.; Wu, T.; Wang, M.; Shi, S.; Yuan, G.; Li, X.; Chong, H.; Wu, B.; Zheng, P. Enzymatic biosynthesis and immobilization of polyprotein verified at the single-molecule level. *Nat. Commun.* **2019**, *10*, 2775. [CrossRef]
66. LeBlanc, M.A.; Fink, M.R.; Perkins, T.T.; Sousa, M.C. Type III secretion system effector proteins are mechanically labile. *Proc. Natl. Acad. Sci. USA* **2021**, *118*, e2019566118. [CrossRef]
67. Hu, X.; Zhao, X.; He, B.; Zhao, Z.; Zheng, Z.; Zhang, P.; Shi, X.; Kwok, R.T.K.; Lam, J.W.Y.; Qin, A.; et al. A simple approach to bioconjugation at diverse levels: Metal-free click reactions of activated alkynes with native groups of biotargets without prefunctionalization. *Research* **2018**, *2018*, 3152870. [CrossRef] [PubMed]
68. Shi, S.; Wang, Z.; Deng, Y.; Tian, F.; Wu, Q.; Zheng, P. Combination of click chemistry and enzymatic ligation for stable and efficient protein immobilization for single-molecule force spectroscopy. *CCS Chem.* **2022**, *4*, 598–604. [CrossRef]
69. Cao, Y.; Lam, C.; Wang, M.; Li, H. Nonmechanical protein can have significant mechanical stability. *Angew. Chem. Int. Ed.* **2006**, *45*, 642–645. [CrossRef] [PubMed]
70. Marko, J.F.; Siggia, E.D. Stretching DNA. *Macromolecules* **1995**, *28*, 8759–8770. [CrossRef]
71. Garg, S.; Singaraju, G.S.; Yengkhom, S.; Rakshit, S. Tailored polyproteins using sequential staple and cut. *Bioconjugate Chem.* **2018**, *29*, 1714–1719. [CrossRef]
72. Tian, F.; Li, G.; Zheng, B.; Liu, Y.; Shi, S.; Deng, Y.; Zheng, P. Verification of sortase for protein conjugation by single-molecule force spectroscopy and molecular dynamics simulations. *Chem. Commun.* **2020**, *56*, 3943–3946.
73. Lv, S.; Dudek, D.M.; Cao, Y.; Balamurali, M.M.; Gosline, J.; Li, H. Designed biomaterials to mimic the mechanical properties of muscles. *Nature* **2010**, *465*, 69–73. [PubMed]
74. Li, H.; Cao, Y. Protein mechanics: From single molecules to functional biomaterials. *Acc. Chem. Res.* **2010**, *43*, 1331–1341. [PubMed]
75. Khoury, L.R.; Slawinski, M.; Collison, D.R.; Popa, I. Cation-induced shape programming and morphing in protein-based hydrogels. *Sci. Adv.* **2020**, *6*, eaba6112. [CrossRef]
76. Hoffmann, T.; Tych, K.M.; Crosskey, T.; Schiffrin, B.; Brockwell, D.J.; Dougan, L. Rapid and robust polyprotein production facilitates single-molecule mechanical characterization of beta-barrel assembly machinery polypeptide transport associated domains. *ACS Nano* **2015**, *9*, 8811–8821.
77. Yang, R.; Wong, Y.H.; Nguyen, G.K.T.; Tam, J.P.; Lescar, J.; Wu, B. Engineering a catalytically efficient recombinant protein ligase. *J. Am. Chem. Soc.* **2017**, *139*, 5351–5358.